Zahn, R., Comas, M.C., and Klaus, A. (Eds.), 1999
Proceedings of the Ocean Drilling Program, Scientific Results, Vol. 161

8. MINERALOGY AND MICROFABRIC OF SEDIMENT FROM THE WESTERN MEDITERRANEAN SEA[1]

Jane S. Tribble[2] and Roy H. Wilkens[2]

ABSTRACT

Analysis of bulk mineralogy and microfabric of sediments collected during Ocean Drilling Program Leg 161 indicates a notably uniform Neogene/Quaternary history of hemipelagic sedimentation in the Western Mediterranean Sea. Bulk X-ray diffraction data were collected for 857 samples from six drill sites in an east–west transect from the Tyrrhenian Sea to the western Alboran Sea. Semiquantitative relative abundances of clay minerals, calcite, quartz, and feldspar are reported. Age profiles of the major phases are used to describe downhole and east–west variations in mineralogy of the dominant hemipelagic sediments. Although overall mineralogy is remarkably similar from site to site, some spatial variability was noted. Calcite content increases from an average of ~20% in the westernmost Alboran Sea to ~40% in the Tyrrhenian Basin. Calculated calcite burial fluxes correlate with sedimentation rates and define an opposite trend, with greatest accumulation rates in the western Alboran Sea. Quartz concentrations are slightly higher in hemipelagic sediments from the westernmost Alboran Sea sites than in the eastern Alboran, Balearic, and Tyrrhenian Basins. These compositional trends are thought to reflect the influence of detrital influx to the basins. Age profiles of calcite flux reveal peaks, many of which correlate between sites. Climate change, with associated changes in delivery of detrital material to the basins, and possibly in productivity, are likely responsible for the peaks in calcite accumulation.

Backscattered electron images of 36 samples of hemipelagic sediment were collected and analyzed for areal percentages of grains, macropores, and matrix. Microfabric samples from a depth profile at Site 974, and across three time slices at all sites, show only minor variations in gross fabric related to age, depth of burial, or location. All samples are matrix dominated. Grains and macropores provide minor contributions to sediment fabric. Porosities calculated for the matrix material correlate well with total sample porosities.

INTRODUCTION

Sites drilled during Ocean Drilling Program (ODP) Legs 160 and 161 form an east–west, trans-Mediterranean transect focused on Mediterranean paleoceanography as well as numerous regional tectonic objectives. The principal paleoceanographic objectives of Leg 161 were to examine environmental conditions that prevailed in the Western Mediterranean Sea during deposition of Pliocene–Pleistocene sapropels in the eastern Mediterranean and to document the Cenozoic history of hydrography and circulation within the western Mediterranean. Tectonic objectives of Leg 161 involved the origin of extensional basins in collisional settings and focused on the formation of the Alboran Basin (Fig. 1).

Site 974 is located in a small basin within the central Tyrrhenian Sea, a backarc basin that opened during late Miocene–Pleistocene times (Fig. 1). It is located ~300 m from Site 652, drilled during Leg 107 (Kastens, Mascle, Auroux, et al., 1987). The Pliocene–Pleistocene sequence at Site 974 consists of hemipelagic sediments (primarily nannofossil to nannofossil-rich clay and silty clay and nannofossil ooze), punctuated by organic-rich layers (lower organic content analogs of the sapropels found throughout the eastern Mediterranean; e.g., Emeis, Robertson, Richter, et al., 1996) and volcaniclastic deposits (McCoy and Cornell, 1990; Comas, Zahn, Klaus, et al., 1996). Site 975 is located on the Menorca Rise on the northern margin of the South Balearic Basin (Fig. 1). Nannofossil to calcareous clays and silty clays typify the Pliocene–Pleistocene hemipelagic sequence recovered at this site (Comas, Zahn, Klaus, et al., 1996). Documentation of organic-rich layers at Site 975 indicates paleoceanographic conditions associated with cyclic deposition of sapropel-like layers extended farther to the west than previously thought (e.g., Emeis et al., 1991). The Pliocene–Pleistocene hemipelagic sediments at Site 975 overlie micrites and evaporites of the latest Miocene (Messinian; see Marsaglia and Tribble, Chap. 1, this volume).

Four sites were drilled across the Alboran Sea to investigate the subsidence histories and tectonic evolutions of the major sub-basins (the Western Alboran Basin [Site 976], the Eastern Alboran Basin [Sites 977 and 978], and the Southern Alboran Basin [Site 979]; Fig. 1). The Alboran Basin formed by extension of continental crust behind arcuate thrust belts that remained active during evolution of the basin; models explaining the origin of extension in an overall collisional setting are numerous and controversial (see discussion in Comas, Zahn, Klaus, et al., 1996). The Alboran Basin has relatively shallow water depths (<2000 m) and contains up to 7 km of sedimentary fill (Comas et al., 1992; Jurado and Comas, 1992). The hemipelagic sediments, sampled during Deep Sea Drilling Project Leg 13 and ODP Leg 161, consist primarily of nannofossil-rich clays and nannofossil to calcareous clays and silty clays (Ryan, Hsü, et al., 1973; Comas, Zahn, Klaus, et al., 1996). In addition to these clay-dominated lithologies, intervals of sand and or gravel of Miocene–Pliocene age were penetrated at Sites 976, 977, and 978. Nearly 260 m of metamorphic basement was penetrated at Site 976.

This study addresses the long-term history of hemipelagic sedimentation in the western Mediterranean through quantitative bulk X-ray mineralogy analyses. In addition, the hemipelagic sediments are characterized by backscattered electron microscope studies of microfabric. The microfabric of a sediment reflects its original mineralogy and depositional environment, postdepositional diagenesis and compaction, and deformation. Changes in a sediment's microfabric are accompanied by changes in physical properties such as porosity, density, and acoustic velocity. In addition to providing a record of the composition and history of a sediment, microfabric is an important determining factor in the response of sediment to compaction and deformation. Digital image analysis is used in this study to quantify as-

[1]Zahn, R., Comas, M.C., and Klaus, A. (Eds.), 1999. *Proc. ODP, Sci. Results*, 161: College Station, TX (Ocean Drilling Program).
[2]School of Ocean and Earth Science and Technology, University of Hawaii, Honolulu, Hawaii 96822, U.S.A. jtribble@soest.hawaii.edu

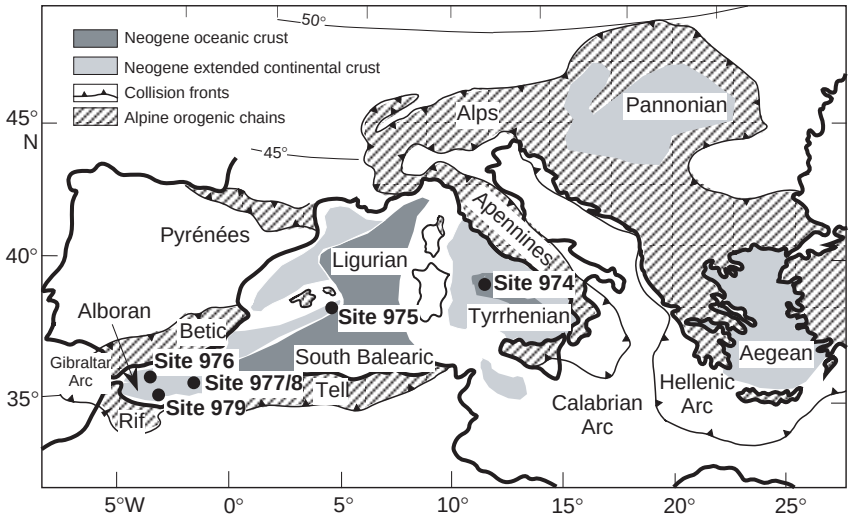

Figure 1. Locations of Leg 161 sites in the Western Mediterranean Sea.

pects of the sediment microfabric, and these data are related to sediment composition and physical properties.

METHODS

Sample Selection

Samples were collected approximately once per section from one hole at each site drilled during Leg 161. During sample selection, emphasis was placed on the dominant lithology of each core (generally hemipelagite); only a few samples of minor lithologies were taken. A total of 857 samples were analyzed for major mineralogy. A subset of 36 of these samples was also imaged with the scanning electron microscope (SEM). Hole 974B was chosen for detailed image analysis, whereas samples ~0.5, 2.0, and 5.0 Ma (nannozones 19F, 19A, and 12, respectively) were taken from each of the other sites so that fabric of sediment deposited across the western Mediterranean during the same period of time could be compared. Almost all of the samples were collected adjacent to a physical properties sample so that imaging and mineralogy data could be compared to measurements of density, porosity, and velocity.

Mineralogy

X-ray diffraction (XRD) was used to determine bulk mineralogy. Samples from Holes 974B, 975B, 976B, 977A, and 978A were analyzed on board ship according to methods described in Shipboard Scientific Party (1996a). Samples from Hole 979A were analyzed at the University of Hawaii (UH) using a Scintag PAD V powder diffractometer. The samples were continuously scanned from 2° to 70° 2θ, using a chopper increment of 0.03° and a scan speed of 1° 2θ/min. Unfiltered Cu Kα radiation was used with a tube voltage of 45 kV and a tube current of 40 mA.

The relative abundances of total clay minerals, quartz, plagioclase, and calcite, normalized to 100%, were estimated for all bulk samples using a routine developed at UH. The routine uses a simultaneous linear equation algorithm that accounts for peak overlap (Karlak and Burnett, 1966) and was calibrated using a series of multicomponent mixtures as external standards. Details of the quantification method are given in Wilkens et al. (1992). Analysis of standard mixtures of clay minerals, quartz, feldspar, and calcite using this quantification routine indicate results are generally good to within 10% of the actual sample composition (Wilkens et al., 1992). Resolution for these phases is on the order of 2% or better. To evaluate how well the quantification algorithm works on the Leg 161 samples, XRD results for calcite and shipboard measurements of carbonate content (Comas, Zahn, Klaus, et al., 1996) are plotted vs. depth in Figure 2. The geochemical analyses tend to be somewhat greater than the XRD results; some of this difference may be a result of the fact that carbonate in the form of dolomite is present in the samples and would have been included in the total carbonate of the shipboard analyses. Although dolomite was not included in the quantification routine, the relative intensity of the main dolomite X-ray peak was determined. This relative intensity is simply a measure of dolomite peak height relative to the most intense peak in the pattern and should not be compared numerically with the weight percentages of clay minerals, calcite, quartz, and feldspar.

Scanning Electron Microscopy

SEM samples were stored in sealed containers with damp sponges to maintain fluid saturation during transport to the laboratory. Within several months of the cruise, 3- to 4-mm-thick slices of the samples chosen for SEM examination were treated to replace their pore fluids with epoxy. Replacement of the pore fluid involves two different exchanges because the Spurr low-viscosity epoxy used is not soluble in water. The exchange process was performed stepwise, soaking samples for 48 hr first in a fluid mixture of 80% water and 20% acetone, and proceeding in 20% steps (60:40, 40:60, 20:80) every two days until the sample was soaking in pure acetone. The process was then repeated using an acetone-epoxy mixture, gradually replacing the acetone in the sediment pores with epoxy. The samples were then cured, cut, polished using 0.25-µm grit, and mounted for study using a backscattered detector in the SEM. The efficacy of the replacement process was confirmed by the fact that internal voids such as those within foraminifer tests were epoxy filled. This process has been repeatedly successful in preserving delicate sediment microfabric (Tribble et al., 1993; Tribble and Wilkens, 1994).

Backscattered electron (BSE) images were collected on a Zeiss DSM 962 SEM at five magnifications (100×, 200×, 500×, 1000×, and 2000×). Digital files of these images are available in Appendix A on CD-ROM, this volume. In these digital images, the intensity of backscattered electrons is directly proportional to density, so that denser objects appear brighter in the captured images, whereas epoxy is black. Relatively large grains appear uniformly light gray to white. Grains are surrounded by matrix of a darker hue comprised of clay-sized grains and microporosity, and relatively large pore spaces (macropores), now filled with epoxy, are black. Digital image analy-

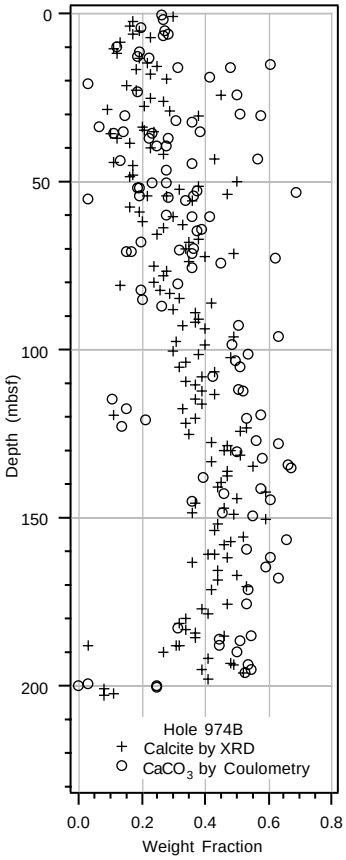

Figure 2. Depth profiles of carbonate content as measured by shipboard coulometric analysis and calcite content as determined by X-ray diffraction for sediment from Hole 974B. Overall agreement of the two data sets is quite good. Offset to higher values of the shipboard carbonate analyses reflects in part inclusion of noncalcite carbonates such as dolomite.

sis was used to quantify the volumes occupied by these three fabric elements (grains, matrix, and macropores) using methods described in Tribble and Wilkens (1994).

DESCRIPTION OF MINERALOGY AND MICROFABRIC

Hemipelagic Sediment

X-ray intensities of major phases are given in Appendix B (CD-ROM, this volume) for all samples analyzed, with the exception of the Miocene section from Site 975; those data are reported in Marsaglia and Tribble (Chap. 1, this volume). X-ray mineralogy results are displayed as cumulative major mineral content vs. age up to 6 Ma in Figure 3. Because older sediments were recovered at Sites 976 and 978, the entire age profiles for those sites are shown separately (Fig. 4). Locations of SEM samples are indicated by circles on the figures. Ages were calculated by linear interpolation between biostratigraphic event markers using data contained in individual site chapters (Comas, Zahn, Klaus, et al., 1996). In addition, average weight percentages of the four major phases, plus the average relative intensity of the dolomite peak, are given in Table 1 for each lithologic unit.

All of the mineralogy profiles are dominated by clay minerals and calcite (Figs. 3, 4). Feldspar is present in only minor amounts in most samples. Quartz averages between 10% and 20% with a few exceptions, most notably in samples near the Pliocene/Pleistocene boundary (2 Ma) at Sites 975 and 976, in the Pleistocene (0.4–0.7 Ma) at Site 974, and in sediments older than 6 Ma at Site 978. Figure 5 illustrates a typical microfabric of the dominant hemipelagic sediments. Our backscattered electron micrographs were collected by imaging flat, polished surfaces; the images thus represent vertical cross sections of sediment structure. The fabric of the hemipelagites is dominated by the medium gray matrix material (a mixture predominantly of clay minerals and microporosity at a scale too fine for resolution in this image; Fig. 5). Quantification of the fabric elements yielded an average value of 91% matrix for this sample. Silt- to sand-sized terrigenous grains (TG, primarily quartz with minor feldspar) and foraminifer fragments (F) appear as bright areas within the darker matrix and total to an average of 9% grains. Most terrigenous grains are <10 μm in diameter. No macropores are visible in this image so the quantified macroporosity was negligible.

Calcite in the hemipelagic sediments is present primarily as biogenic particles (primarily nannofossils and foraminifers). Abundant and well-preserved foraminifers are evident in images of many samples, especially those from more eastern sites (e.g., Sample 161-974B-6H-7, 39 cm; Fig. 6). The foraminifer tests are generally not filled with matrix material, a condition that tends to increase total porosity of the sediment. Interestingly, these tests often remain empty of matrix material to depths of hundreds of meters and only begin to fill when recrystallization of calcite and biogenic silica begins (Wilkens et al., 1987). In Figure 6, some of the epoxy has been plucked from inside the tests during polishing, but it appears that most tests are epoxy filled and did not contain matrix. This sample has a relatively high carbonate content (47% from XRD), as do many of the samples below it, and is fairly typical of the hemipelagic sediments from Sites 974 and 975.

There is an east–west trend of decreasing calcite abundance in the hemipelagic sediments (Fig. 3; Table 1), from ~40% in the Balearic and Tyrrhenian Seas, to ~20% calcite in the western Alboran Sea. Although present, foraminifers are less abundant in sediments of the Alboran Sea, compared to the eastern sites (Sites 974 and 975). Figure 7 illustrates the fabric of a typical western Alboran sample that contains ~22 wt% calcite by XRD. Coccoliths, although not individually visible at the scale of this image, make up the bulk of the carbonate content. This sample also contains abundant quartz (16 wt% by XRD).

Calcite contents of western Alboran sediments (Holes 976B and 979A) do not change appreciably with age (Fig. 3; Table 1). In the Eastern Alboran Sea (Holes 977A and 978A), Balearic Sea (Hole 975B), and the Tyrrhenian Sea (Hole 974B), calcite content tends to decrease with decreasing age of the sediment (Fig. 3; Table 1). The greatest concentrations of carbonate occur at Site 974 in sediments between 3 and 4.5 m.y. old. The greater abundance of carbonate in the older sediments does not appear to reflect higher concentrations of foraminifer tests. We analyzed all of the Hole 974B images (~300; see Appendix A) and observed no increase in the average number of grains per image in the older samples. However, higher magnification revealed a large component of carbonate in the matrix in the form of coccolith platelets (Fig. 8).

To obtain a better understanding of spatial and temporal differences in calcite content, calcite fluxes were calculated for each site (where data were available) according to the following:

$$\text{flux} = \text{wt. fract.} \times \text{sed. rt.} \times \text{BD} \times (1 - \text{por}),$$

where the flux is calculated in g $CaCO_3/cm^2$/m.y., wt. fract. is the weight fraction of calcite in the sediment as determined by XRD, sed. rt. is the sedimentation rate in cm/m.y. calculated from shipboard determinations of biostratigraphic events (see individual site chapters in Comas, Zahn, Klaus, et al., 1996), BD is the bulk density of each sample in g/cm^3, and (1 – por) is the fraction of grains, cal-

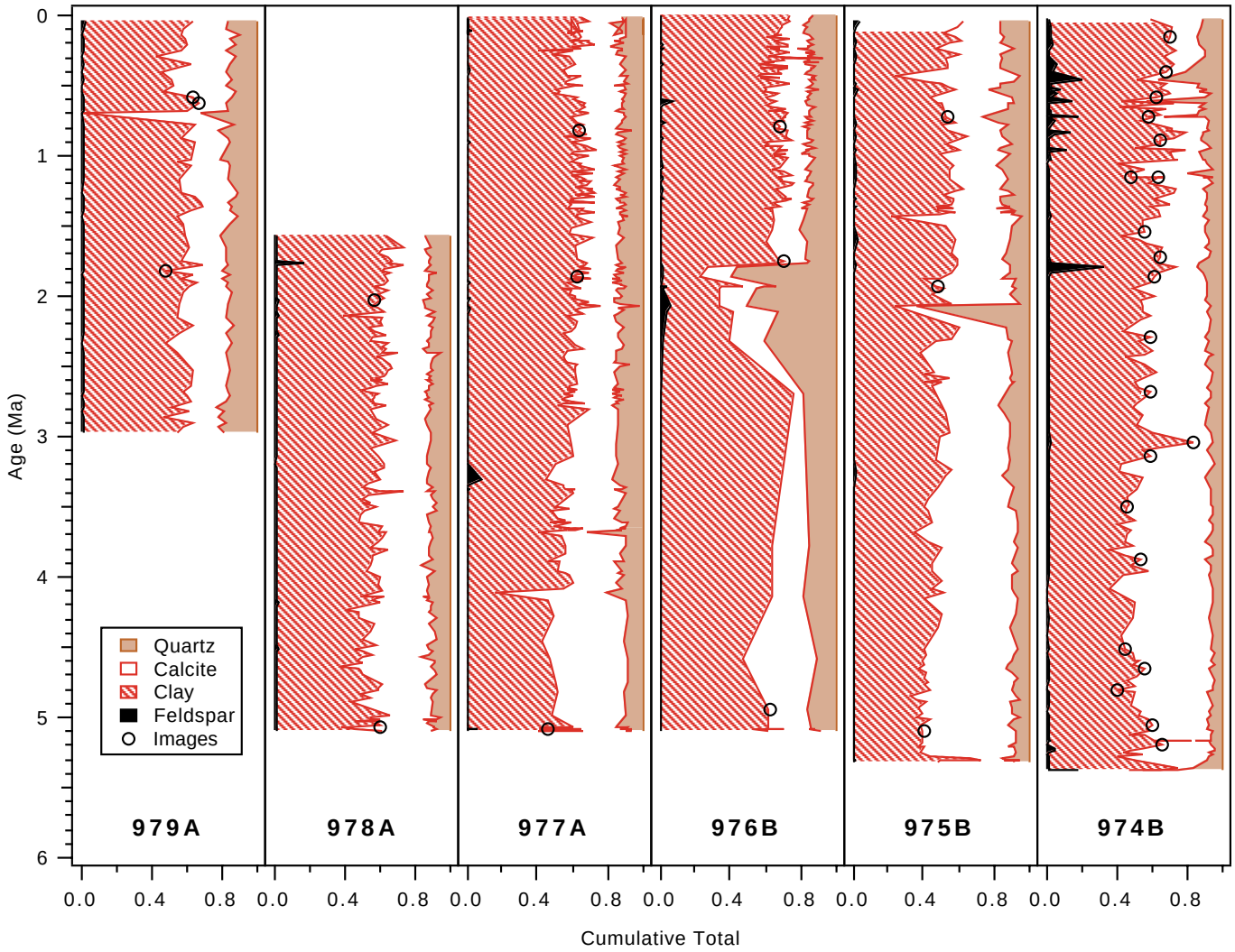

Figure 3. Cumulative plots of bulk mineralogy vs. age up to 6 Ma for each of the Leg 161 sites. Location of microfabric samples are indicated by circles on the plots.

culated as 1 minus the fractional porosity. Bulk density and porosity data are available for samples taken adjacent to nearly all of our samples (Comas, Zahn, Klaus, et al., 1996). The resulting flux data (Fig. 9) represent the net burial of calcite and thereby reflect the balance of delivery of calcite to the site and possible dissolution of calcite. Periods of high flux may represent times of relatively high calcite productivity in surface waters, times of general high sedimentation rate during which detrital carbonate is delivered to the site, times of particularly low calcite dissolution, or any combination thereof.

A generally west–east trend of decreasing calcite flux is apparent (Fig. 9). Note that this trend is opposite to that defined by the calcite content data (Fig. 3; Table 1). Interestingly, the average calcite flux data for each site are correlated with current water depths of the sites (Table 2). This is true whether all flux data from each site are averaged, or whether a background flux average is determined by eliminating peaks from the calculation. Although Mediterranean bottom waters are currently supersaturated with respect to calcite and aragonite (Millero et al., 1979; Takahashi et al., 1980), dissolution of calcite within the sediment column driven by organic matter degradation is possible (e.g., Archer et al., 1989). Background concentrations of total organic carbon for the easternmost sites are low, despite the isolated high values found in organic-rich layers (see Sites 974 and 975 chapters in Comas, Zahn, Klaus, et al., 1996). It is likely, therefore, that dissolution of carbonate plays at most a minor role. The overall west–east trend of decreasing calcite flux more likely reflects higher delivery rates of calcite to the westernmost sites.

It is not possible from the XRD data alone to determine whether the calcite flux values indicate a trend of decreasing carbonate productivity from west to east, or whether the flux values primarily reflect detrital input rates. If the detrital sediment delivered to the Alboran Sea contains a significant fraction of carbonate, calcite flux rates would be high, although the percentage of calcite in the sediment could still be relatively low because of dilution by the noncarbonate fraction of the detrital sediment. The inverse correlation of calcite flux with water depth across the six sites (Table 2) may reflect the greater distance of deeper sites from shallow shelves that could provide a source of detrital carbonate. Our microfabric images of the western Alboran sediments typically show abundant silt- to clay-sized grains, many of which appear from backscattered electron in-

tensities to be carbonate (e.g., Fig. 10). These grains are generally rounded and show no obvious biogenic morphology or structure, which indicates a likely detrital origin.

The age profiles of calcite flux (Fig. 9) indicate no overall temporal change in flux, except at Site 977 where sediments younger than 1.5 Ma are characterized by somewhat higher calcite fluxes than the older sediments. Each profile, however, is characterized by peaks of calcite flux above relatively uniform background flux levels for each site. Temporal correlations of some of these peaks from site to site (Fig. 9) indicate the regional nature of the causal events, whether they were high productivity events or times of increased detrital flux of calcite. Comparison of BSE images of high and low calcite flux samples shows no consistent difference in the ratio of biogenic to detrital carbonate. Temporal correlations of peaks in carbonate content of the fine-grained fraction (<20 µm) of samples from the Alboran Sea sites have also been noted by Skilbeck and Tribble (Chap. 7, this volume). The lack of similar correlation in abundance of fine detrital quartz, and the frequency of the peaks (roughly every 0.5 Ma), lead them to postulate a climatic control on carbonate productivity as a causal factor. The magnitudes of the calcite flux peaks calculated in this study, however, suggest that detrital input of carbonate to the sites is important. The background flux levels are comparable to the upper range of open ocean values of calcite mass accumulation rates (Farrell and Prell, 1991). To accredit the order-of-magnitude increases in calcite flux observed in the Alboran and Balearic Seas to increased productivity alone would be difficult.

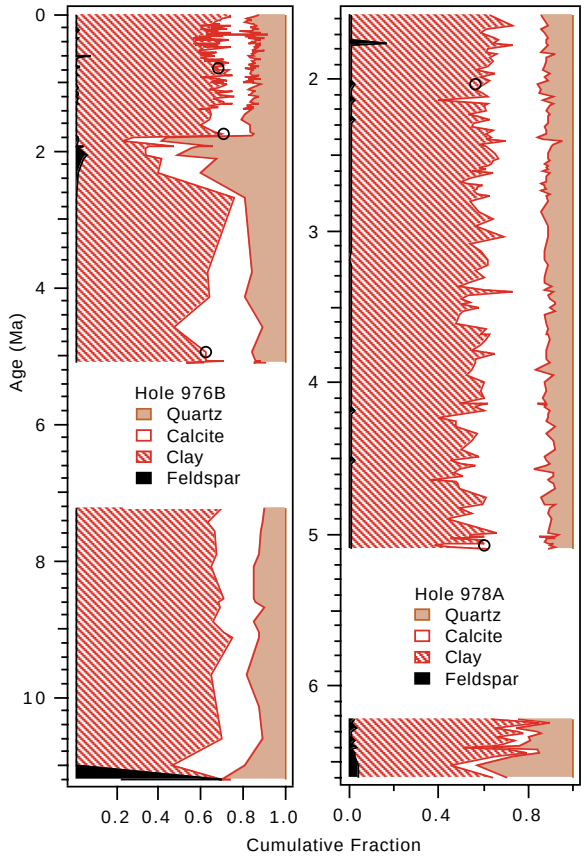

Figure 4. Cumulative plots of bulk mineralogy vs. age for Holes 976B and 978A.

The ~0.4- to 0.5-m.y. frequency of the peaks in calcite flux (Fig. 9) is similar to cyclicity observed in marine carbonates from a variety of settings, generally attributed to dissolution (e.g., Moore et al., 1982; Droxler et al., 1990; Bassinot et al., 1994). The correspondence of this frequency with the 0.413-m.y. period of Earth's eccentricity cycle has been noted, and a direct or indirect connection with global climate inferred, by these authors.

Although the role of dissolution in production of the western Mediterranean carbonate cycles cannot be totally discounted, it seems likely that the primary causative factors were increased delivery of detrital carbonate to the basins, perhaps accompanied by pulses in productivity.

Quartz abundances of hemipelagic sediments are fairly uniform across all six sites (Fig. 3; Table 1), although western Alboran sites are perhaps a little richer in quartz. In the Tyrrhenian Basin (Hole 974B), spikes of high quartz and feldspar content characterize the Pleistocene sediments (Fig. 3). Microfabric examination of a sample corresponding to one of these peaks showed no increase in abundance of large terrigenous grains in images collected at low magnifications. At higher magnification, however, abundant grains under 10 µm are apparent (Fig. 11). It is possible that these grains may have been windborne and that the quartz and feldspar peaks may have paleoclimatologic significance. The three largest peaks of quartz abundance all correlate with spikes in feldspar content, but not all samples with

Table 1. Leg 161 bulk mineralogy: average values for lithologic units.

Hole	Lithologic unit	Depth (mbsf)	Sediment type	Clay minerals (wt%)	Quartz (wt%)	Feldspar (wt%)	Calcite (wt%)	Dolomite (relative intensity)
976B	I	0-362.1	Hemipelagite	66	15	1	18	11
	II	362.1-518.3	Sand and clay	40	40	2	18	47
	III	518.3-660.2	Hemipelagite	64	14	1	21	9
	IV	660.2-669.73	Basal sands	32	25	31	12	39
979A	I	0-580.9	Hemipelagite	57	17	1	26	5
977A	IA	0-417.4	Hemipelagite	61	13	1	25	9
	IB	417.4-490.8	Hemipelagite	53	14	1	32	6
	IC	490.8-532.9	Hemipelagite	49	10	1	40	3
978A	IA	213.0-342.2	Hemipelagite	60	12	1	27	10
	IB	342.2-409.3	Hemipelagite	57	12	1	30	9
	IC	409.3-620.9	Hemipelagite	53	11	1	35	4
	II	620.9-630.67	Pebbles	—	—	—	—	—
	III	630.67-694.3	Sand/silt/clay	66	23	2	9	9
975B	I	0-305.2	Hemipelagite	48	12	1	40	4
	II	305.2-307.0	Micrite and silty clay	41	13	1	45	13
974B	I	0-88.9	Hemipelagite	60	12	3	25	6
	II	88.9-199.55	Hemipelagite	51	7	1	41	2
	III	199.55-203.86	Clay/silt/sand	55	29	7	9	8

Note: Sites are in order from west to east. — = no data.

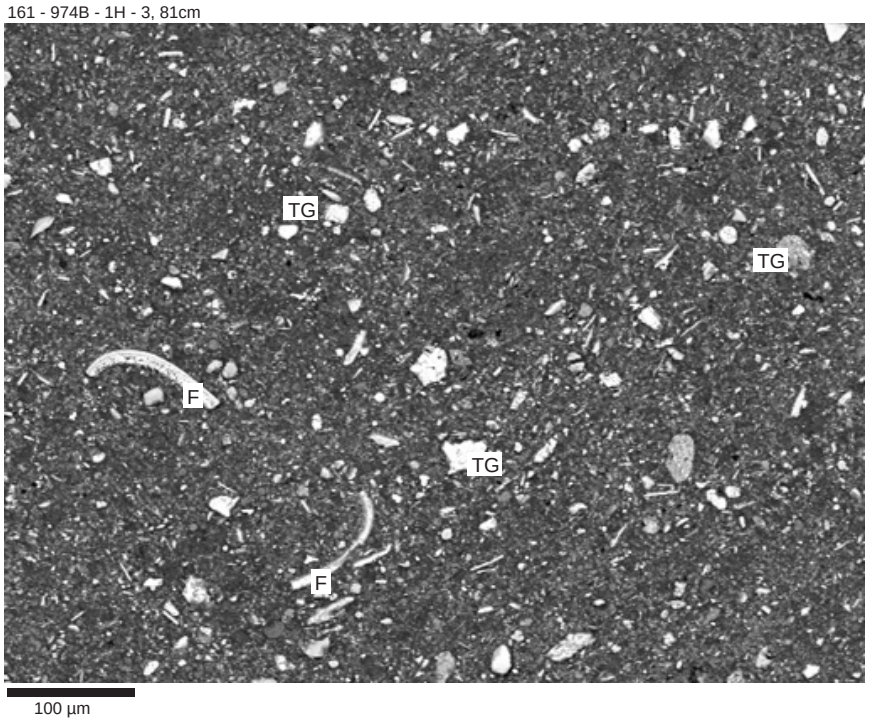

Figure 5. BSE image of Sample 161-974B-1H-3, 81 cm (3.81 mbsf), collected at 200×. Bright (more dense) objects are either foraminifer fragments (F) or terrigenous grains (TG). The bulk of the sample is the matrix of clay minerals and microporosity, with admixed nannofossils.

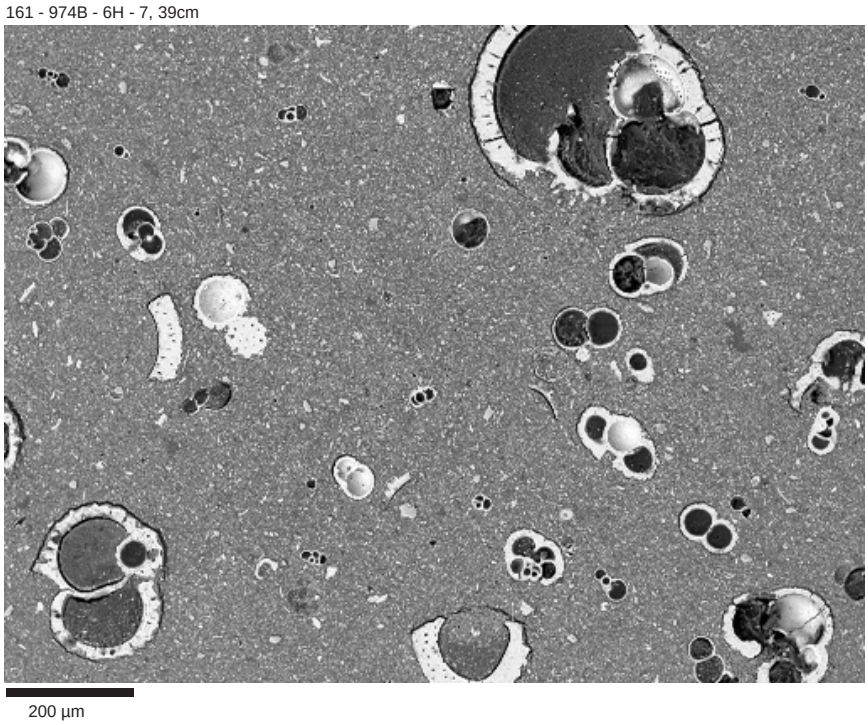

Figure 6. BSE image of a foraminifer-rich sample from the Tyrrhenian Sea (Sample 161-974B-6H-7, 39 cm; 53.89 mbsf; collected at 100×). This carbonate-rich sample contains abundant, well-preserved foraminifers typical of most of the sediments from Holes 974B and 975B.

high percentages of feldspar are enriched in quartz (Fig. 3). Several of the feldspar spikes correspond to samples taken from ash layers as identified visually by shipboard scientists (Shipboard Scientific Party, 1996b, table 4). The elevated quartz contents of some of these layers may reflect entrainment of detrital material during emplacement of the ash layers by gravity flow (a common depositional mechanism for ash layers in the Tyrrhenian Sea; McCoy and Cornell, 1990). Other than the spikes of high feldspar content at Hole 974B, feldspar concentrations of hemipelagic sediments are uniformly low.

Dolomite is present at all sites (Table 1). XRD identification of this phase is tentative; some dolomite is iron-rich and may actually be ankerite. Background levels of dolomite in hemipelagic sediments tend to decrease from west to east, possibly in conjunction with the decrease in sedimentation rates. A detrital source of much of the dolomite was suggested by shipboard scientists (Comas, Zahn, Klaus, et al., 1996).

SAND-RICH INTERVALS

Core recovery of sand-rich intervals was limited, but 27 samples of sandy sediment from Sites 976 and 978 were analyzed for bulk

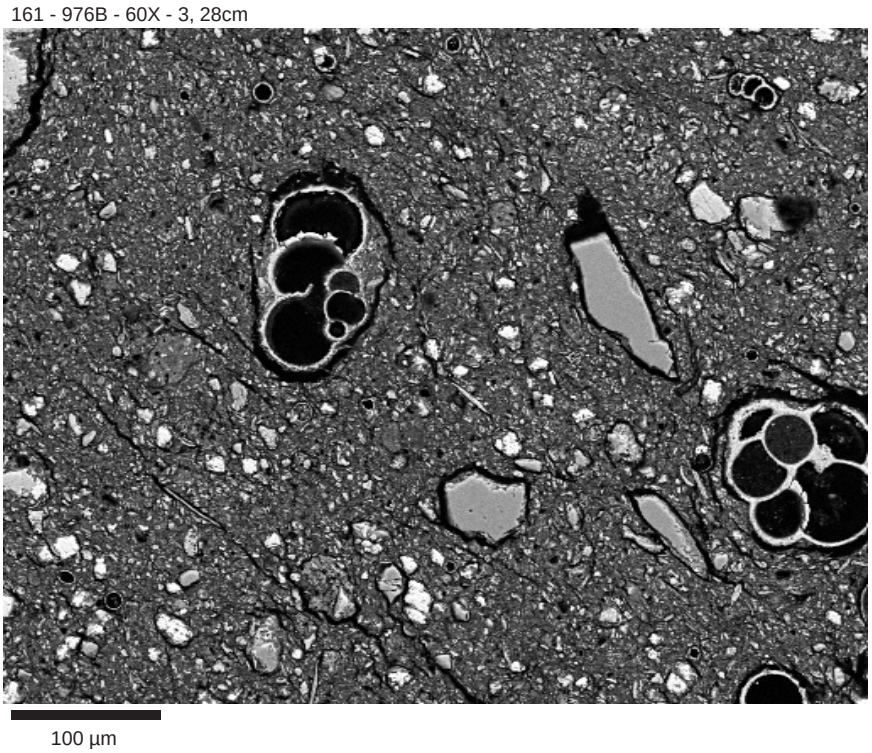

Figure 7. BSE image of a typical hemipelagic sediment from the western Alboran Sea (Sample 161-976B-60X-3, 28 cm; 556.41 mbsf; collected at 200×). Lower calcite content at this site relative to more eastern sites is evident in the lower abundance of foraminifers and nannofossils.

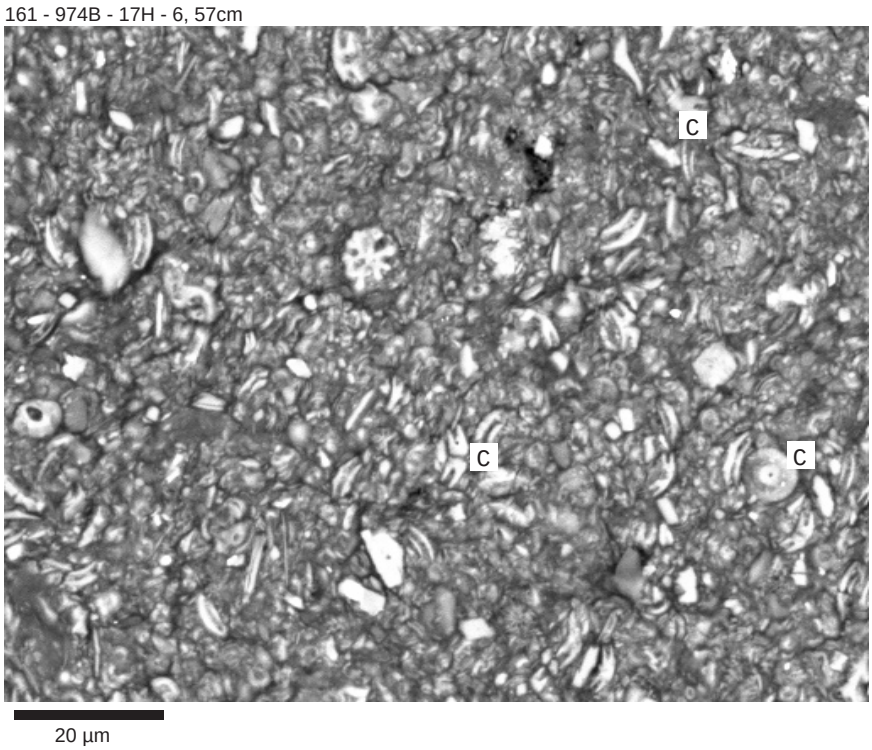

Figure 8. BSE image of a hemipelagic sediment from the Tyrrhenian Sea (Sample 161-974B-17H-6, 57 cm; 157.07 mbsf; collected at 1000×). Coccolith plates (C) dominate the matrix of this carbonate-rich sample.

mineralogy. Pliocene sand-rich lithologies encountered at Site 976 (lithostratigraphic Unit II; see Fig. 4, Table 1) are enriched in dolomite and quartz. The lower half of this unit also contains feldspar concentrations above background levels. Calcite abundances in this sandy unit are similar to those of adjacent hemipelagic sediments, which indicates a likely detrital source for some of the carbonate. One SEM sample was taken from the top of the lithostratigraphic Unit II sandy interval in Hole 976B (Fig. 12). Note the abundance of silt-sized grains and the breakage of the foraminifers. Higher sedimentation rates at Site 976 led to deeper burial and greater compaction than noted in a stratigraphically equivalent sample from the Balearic Basin (Hole 975B; Fig. 13). Basal sediments at Site 976 are enriched in quartz, feldspar, and dolomite relative to the shallower hemipelagic sediments (Fig. 4; Table 1). In contrast to the sand-rich intervals of Site 976, the sand-rich unit (lithostratigraphic Unit III) of Miocene age at the base of Hole 978A is marked by an increase in terrigenous sediment (quartz, clay minerals, and feldspar) and dolomite at the expense of calcite (Table 1).

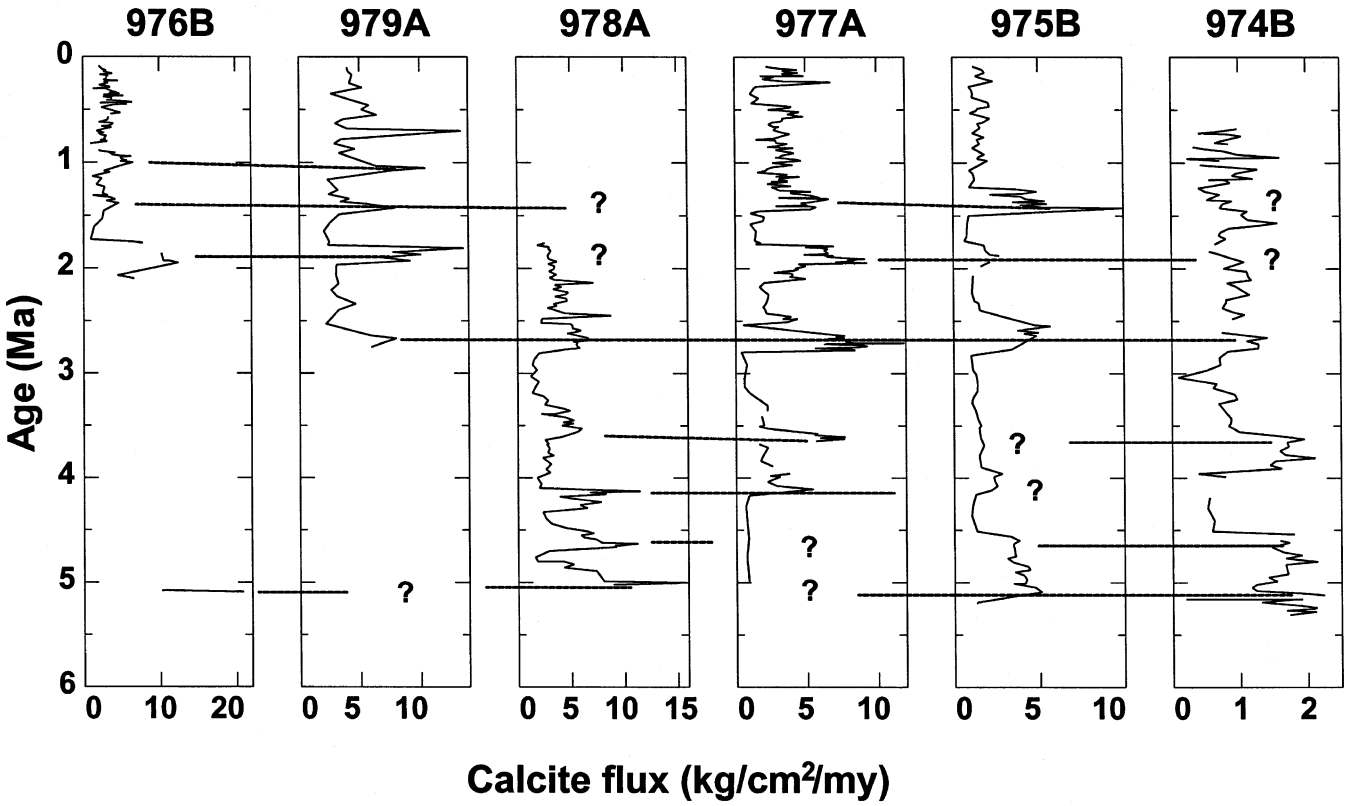

Figure 9. Calcite flux plotted vs. age for all six Leg 161 sites, arranged from west to east. Gaps in the data reflect incomplete core recovery, lack of physical properties measurements, or incomplete sedimentation rate data, usually because of hiatuses in the section.

Table 2. Average calcite flux and sedimentation rate data.

Site	Water depth (m)	Average calcite flux ($kg/cm^2/m.y.$)	Average background flux ($kg/cm^2/m.y.$)	Average Pleistocene sedimentation rate (m/m.y.)	Average upper Pliocene sedimentation rate (m/m.y.)
976	1108	4.1	3.0	208	340
979	1062	5.0	3.7	200	187
978	1929	4.6	3.1	127	111
977	1984	3.9	2.8	154	96
975	2417	2.5	1.5	68	48.9
974	3459	1.1	0.8	55	27.2

Note: Average Pleistocene and upper Pliocene sedimentation rates are from individual site chapters (Comas, Zahn, Klaus, et al., 1996).

ASH LAYERS

Although our emphasis in this study was on analysis of dominant lithologies, we selected two ash layers from the Tyrrhenian Sea (Site 974) for microfabric analysis. A sample of vitric ash (Sample 161-974B-2H-3, 76 cm; Fig. 14) contains abundant volcanic glass. Most of the glass shards are still intact, although some of the grains appear to be undergoing corrosion. Note the near absence of biogenic carbonate (XRD calcite content is 11%), probably because the relatively rapid deposition of the glass swamped any pelagic carbonate contribution to the sediment composition. Alignment of the glass shards is evident; unfortunately, although orientation of all BSE samples relative to vertical was recorded, this sample broke into several pieces during impregnation, and orientation of the pieces is indeterminable. An altered volcanic ash sample from greater depth in Hole 974B was also imaged (Sample 161-974B-13-6, 83 cm; Fig. 15). In this sample the glass has dissolved away leaving voids that are now epoxy-filled. Compare the shapes of the empty casts with glass grains illustrated in Figure 14. This fabric is similar to that noted in previous studies of ash-rich sediments from the Nankai Trough and Hawaiian Arch (Tribble et al., 1993; Tribble and Wilkens, 1994). Maintenance of large, open pores at this burial depth (118 m below seafloor [bsf]) requires that the clay matrix has developed some strength and rigidity (or, less likely in this case, that the pores are overpressured).

QUANTIFICATION OF MICROFABRIC

Quantification of the fabric elements—grains, macropores, and matrix—yielded no significant depth trends and no strong correlations with either mineralogy or physical properties. The percentage of grains, generally <10%, is weakly correlated with the sum of quartz + feldspar. Although foraminifers are visually striking in some samples, the lack of correlation between abundance of grains and the percentage of calcite reflects the dominant contribution of nannofossils to the calcite component. Macropores make a minor contribution to total porosity (<5% in most samples) and show no depth variation in abundance. The few samples with >5% macropores contain abun-

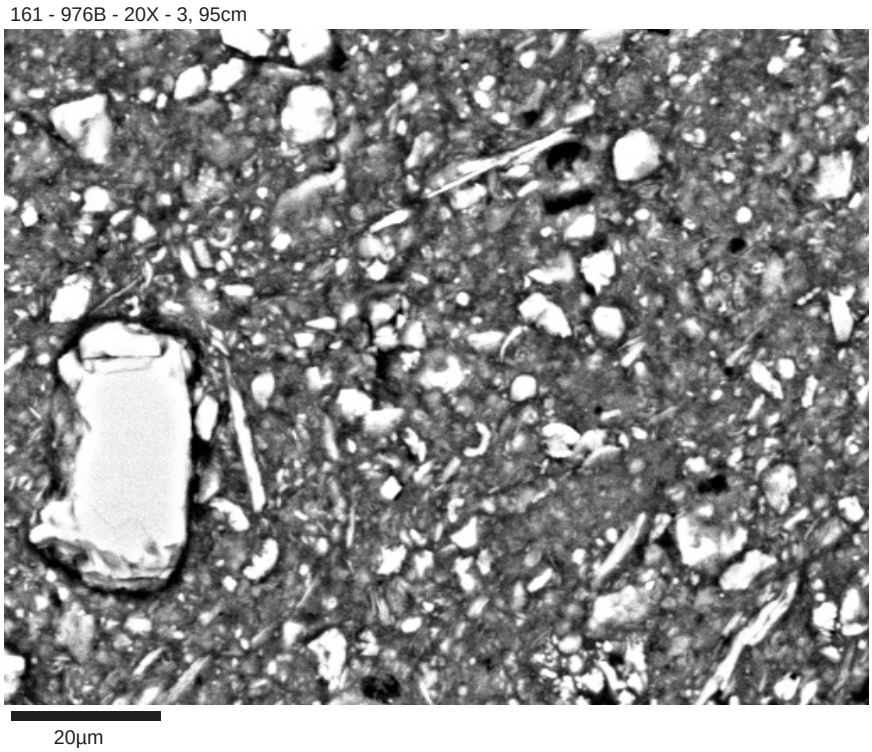

Figure 10. BSE image of a silt-rich sediment from the western Alboran Sea (Sample 161-976B-20X-3, 95 cm; 179.05 mbsf; collected at 1000×). This sample contains abundant silt-sized detrital grains, the brightest of which are thought to be primarily calcite.

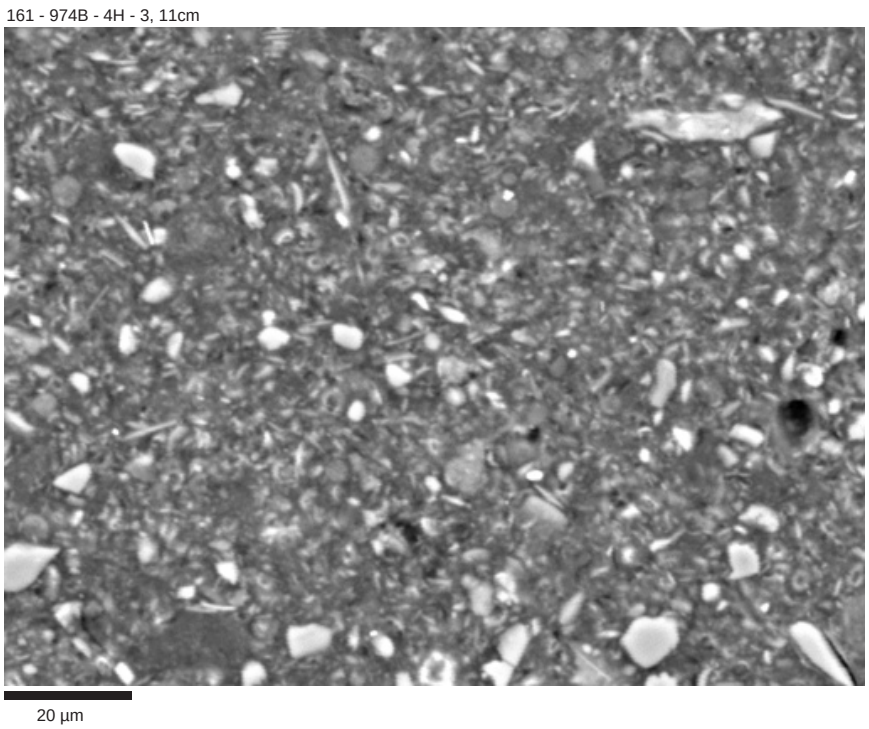

Figure 11. BSE image of Sample 161-974B-4H-3, 11 cm (28.61 mbsf), collected at 1000×. This sample, from one of the quartz peaks in Figure 3, has abundant fine silt- and clay-sized grains of quartz.

dant foraminifers, which indicates the contribution of intratest porosity. The hemipelagic sediments imaged are matrix dominated. Matrix porosity can be calculated from our quantitative data as the difference between total sample porosity and macroporosity divided by the fractional area occupied by matrix. Matrix porosity for samples from Hole 974B approximates well the total porosity of the samples as measured on board ship (Fig. 16). The observed decrease in porosity with burial depth reflects loss of microporosity within the matrix via compaction, with virtually no contribution of loss of macropores.

CONCLUSIONS

The mineralogy of hemipelagic sediments from all sites is dominated by clay minerals and calcite. Quartz and feldspar concentrations in the hemipelagic sediment are relatively low. Calcite content increases somewhat with depth at all sites except the westernmost two (Sites 976 and 979). There is a west–east trend of increasing calcite content of hemipelagic sediments from ~20% in the western Alboran Sea to ~40% in the Balearic and Tyrrhenian Seas, although cal-

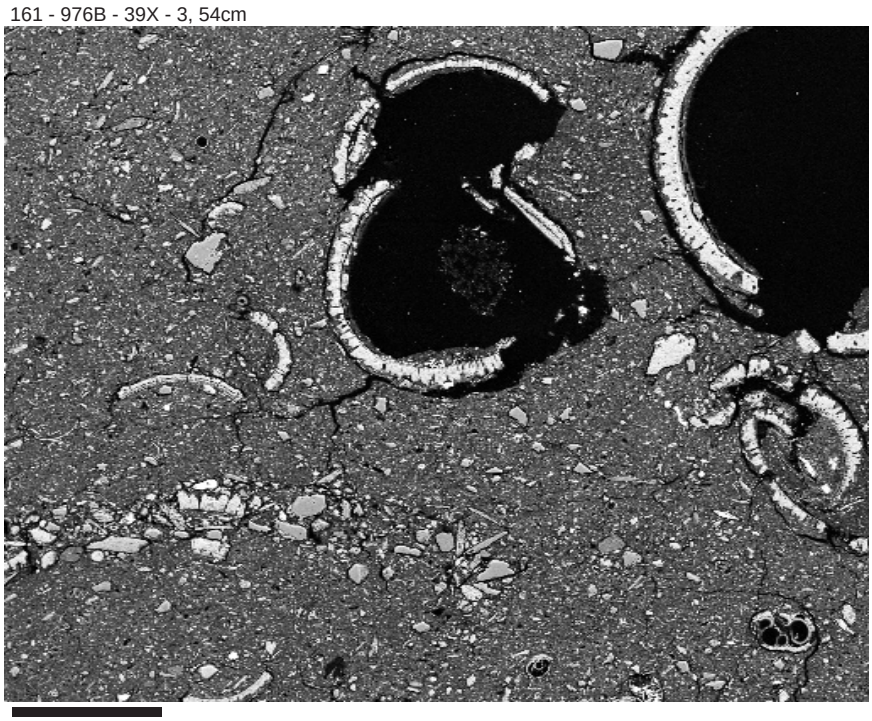

Figure 12. BSE image of Sample 161-976B-39X-3, 54 cm (361.24 mbsf), collected at 100×. Foraminifers and silt-sized quartz and calcite grains are abundant in this ~2.0-Ma sample from the western Alboran Sea. Many of the foraminifer tests are broken because of compaction during burial, but it is only after the tests were substantially crushed that they were filled in with matrix material.

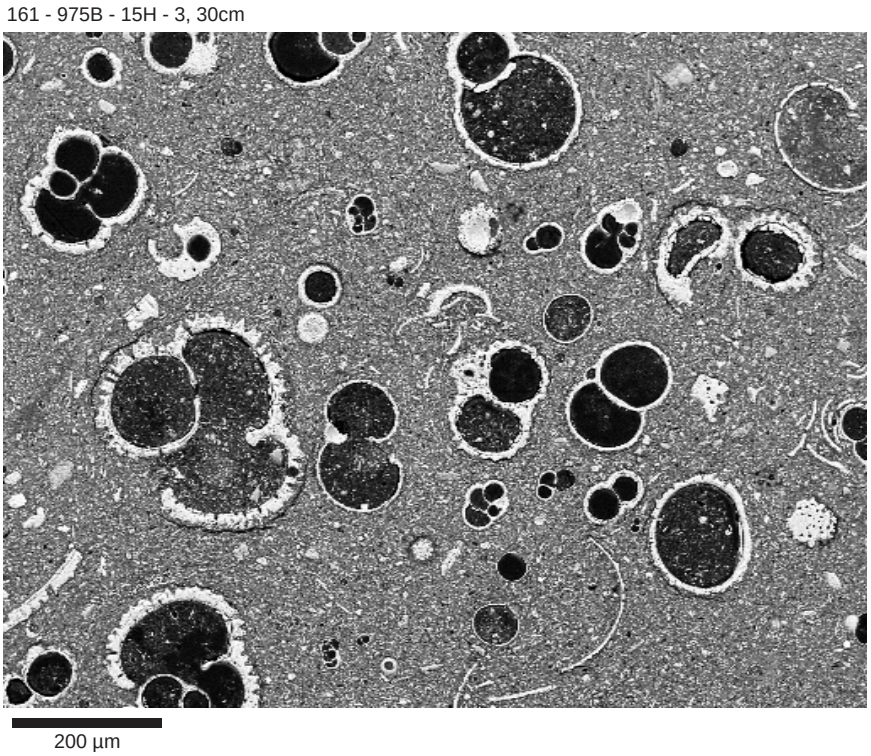

Figure 13. BSE image of Sample 161-975B-15H-3, 30 cm (131.94 mbsf), collected at 100×. Abundant, well-preserved foraminifers are present in this ~2.0-Ma sample from the Balearic Sea. Most foraminifer chambers are empty or contain minor amounts of matrix material. Compare to Figure 12.

culations of calcite flux indicate an opposite trend of decreasing calcite accumulation rates from west to east.

Although our sampling frequency is rather coarse (generally 3 samples per core for bulk mineralogy) compared to most studies of paleoceanography, pulses of calcite flux (mass accumulation rate) have been identified at all western Mediterranean sites. The frequency of these flux peaks (~0.4–0.5 m.y.) is similar to that of carbonate dissolution cycles noted globally (e.g., Moore et al. 1982; Droxler et al., 1990; Bassinot et al., 1994), but the magnitude and character of the Mediterranean flux peaks differ from the fluctuations attributed to dissolution. The calcite flux peaks at the western Mediterranean sites are as much as an order of magnitude greater than background flux levels. In addition, the calcite flux variations of this study appear as peaks above relatively constant background flux levels rather than

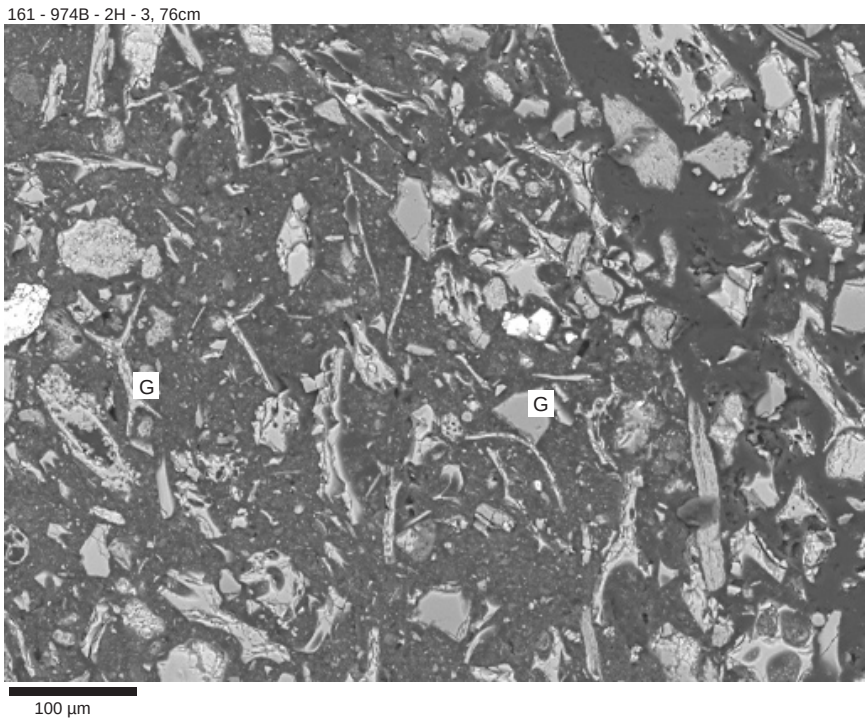

Figure 14. BSE image of a vitric ash sample from the Tyrrhenian Basin (Sample 161-974B-2H-3, 76 cm; 10.26 mbsf; collected at 200×). Grains of volcanic glass (G) show a net alignment.

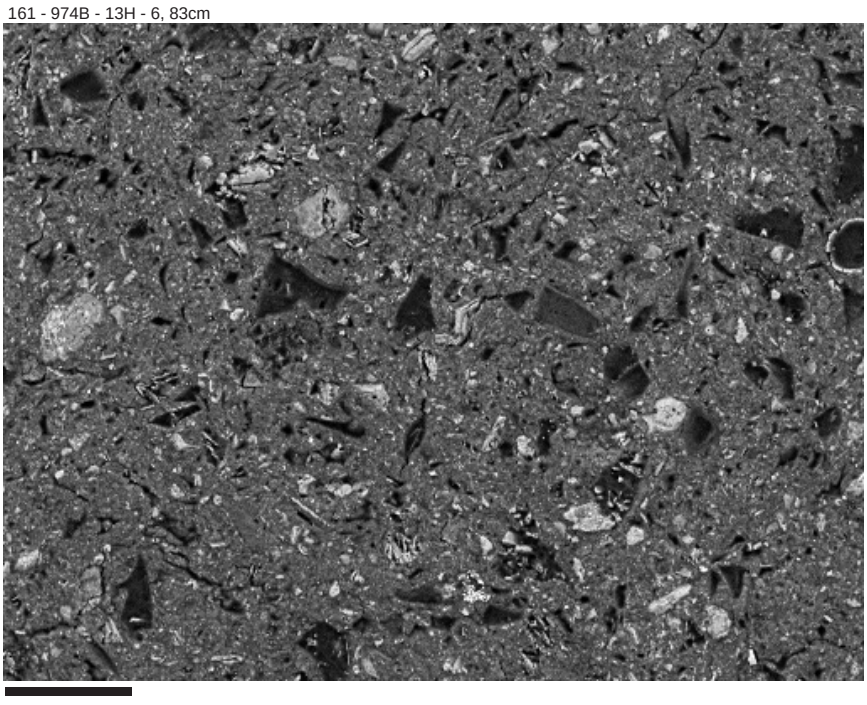

Figure 15. BSE image of an altered ash sample from the Tyrrhenian Basin (Sample 161-974B-13H-6, 83 cm; 119.33 mbsf; collected at 200×). The glass grains of this altered ash have dissolved away, leaving shard-shaped pores. Some of these pores are partially filled by crystal growth, probably of zeolites.

true "cycles." Although a complete explanation of the patterns of calcite accumulation in the western Mediterranean is beyond the scope of this study, it appears likely that influx of detrital carbonate plays a significant role. Potential variations in productivity may also be important. Climate change, with associated changes in runoff, nutrient delivery to the basins, and atmospheric dust fluxes, is the likely driving force behind both the detrital input and productivity variations.

Microfabric of the hemipelagic sediments is dominated by a clay-mineral-rich matrix. Quantifiable grains generally constitute <10% of the area examined. Quartz and, to a lesser extent, feldspar and foraminifers are the major types of grains identified. Macropores make a minor contribution to total sample porosity (generally <5%). Most macropores are associated with foraminifer tests that were not filled in by matrix material.

Although microfabric quantification has proven a useful tool in understanding the ties between compositional and physical properties changes in sedimentary sequences in other studies (e.g., Ehrlich et al., 1984; Ross and Ehrlich, 1991; Tribble and Wilkens, 1994), the rela-

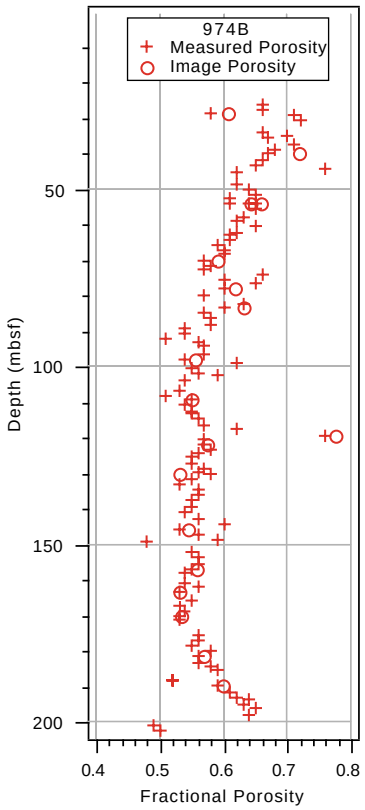

Figure 16. Depth trends of shipboard total porosity measurements and the calculated values for matrix porosity derived from quantitative image analysis. Shipboard porosity was measured on samples immediately adjacent to the microfabric samples. The close correspondence of the matrix porosity data and the total porosity measurements reflects the minor contribution that large pore space (macropores) makes to total porosity in these sediments.

tive homogeneity of the western Mediterranean hemipelagic sequences yielded a notable lack of trends in the microfabric data. The correlation between calculated matrix porosities and total sample porosities as measured on shipboard was the single exception and reflects the dominance of the clay matrix.

ACKNOWLEDGMENTS

The authors would like to thank Marianne Cusimano for tireless work in the XRD laboratory of the *JOIDES Resolution*, Jack Kronen for assistance in image collection, and Yonat Swimmer for data analysis. This work was supported by grants to both authors from the United States Science Advisory Committee.

REFERENCES

Archer, D., Emerson, S., and Reimers, C., 1989. Dissolution of calcite in deep-sea sediments: pH and O_2 microelectrode results. *Geochim. Cosmochim. Acta*, 53:2831–2845.

Bassinot, F.C., Beaufort, L., Vincent, E., Labeyrie, L.D., Rosteck, F., Müller, P.J., Quidelleur, X., and Lancelot, Y., 1994. Coarse fraction fluctuations in pelagic carbonate sediments from the tropical Indian Ocean: a 1,500 kyr record of carbonate dissolution. *Paleoceanography*, 9:579–600.

Comas, M.C., García-Dueñas, V., and Jurado, M.J., 1992. Neogene tectonic evolution of the Alboran Basin from MCS data. *Geo-Mar. Lett.*, 12:157–164.

Comas, M.C., Zahn, R., Klaus, A., et al., 1996. *Proc. ODP, Init. Repts.*, 161: College Station, TX (Ocean Drilling Program).

Droxler, A.W., Haddad, G.A., Mucciarone, D.A., and Cullen, J.L., 1990. Pliocene–Pleistocene aragonite cyclic variations in Holes 714A and 716B (The Maldives) compared with Hole 633A (The Bahamas): records of climate-induced $CaCO_3$ preservation at intermediate water depths. *In* Duncan, R.A., Backman, J., Peterson, L.C., et al., *Proc. ODP, Sci. Results*, 115: College Station, TX (Ocean Drilling Program), 539–577.

Ehrlich, R., Crabtree, S.J., Kennedy, S.K., and Cannon, R.L., 1984. Petrographic image analysis 1, analysis of reservoir complexes. *J. Sediment. Petrol.*, 54:1365–1376.

Emeis, K.-C., Camerlenghi, A., McKenzie, J.A., Rio, D., and Sprovieri, R., 1991. The occurrence and significance of Pleistocene and Upper Pliocene sapropels in the Tyrrhenian Sea. *Mar. Geol.*, 100:155–182.

Emeis, K.-C., Robertson, A.H.F., Richter, C., et al., 1996. *Proc. ODP, Init. Repts.*, 160: College Station, TX (Ocean Drilling Program).

Farrell, J.W., and Prell, W.L., 1991. Pacific $CaCO_3$ preservation and $\delta^{18}O$ since 4 Ma: paleoceanic and paleoclimatic implications. *Paleoceanography*, 6:485–498.

Jurado, M.J., and Comas, M.C., 1992. Well log interpretation and seismic character of the Cenozoic sequence in the Northern Alboran Sea. *Geo-Mar. Lett.*, 12:129–136.

Karlak, R.F., and Burnett, D.S., 1966. Quantitative phase analysis by X-ray diffraction. *Anal. Chem.*, 38:1741–1745.

Kastens, K.A., Mascle, J., Auroux, C., et al., 1987. *Proc. ODP, Init. Repts.*, 107: College Station, TX (Ocean Drilling Program).

McCoy, F.W., and Cornell, W., 1990. Volcaniclastic sediments in the Tyrrhenian Basin. *In* Kastens, K.A., Mascle, J., et al., *Proc. ODP, Sci. Results*, 107: College Station, TX (Ocean Drilling Program), 291–305.

Millero, F.J., Morse, J.W., and Chen, C.-T., 1979. The carbonate system in the western Mediterranean Sea. *Deep-Sea Res.*, 26A:1395–1404.

Moore, T.C., Jr., Pisias, N.G., and Dunn, D.A., 1982. Carbonate time series of the Quaternary and late Miocene sediments in the Pacific Ocean: a spectral comparison. *Mar. Geol.*, 46:217–233.

Ross, C.M., and Ehrlich, R., 1991. *Objective Measurement and Classification of Microfabrics and their Relationship to Physical Properties:* New York (Springer-Verlag).

Ryan, W.B.F., Hsü, K.J., et al., 1973. *Init. Repts. DSDP*, 13 (Pts. 1 and 2): Washington (U.S. Govt. Printing Office).

Shipboard Scientific Party, 1996a. Explanatory notes. *In* Comas, M.C., Zahn, R., Klaus, A., et al., *Proc. ODP, Init. Repts.*, 161: College Station, TX (Ocean Drilling Program), 21–49.

Shipboard Scientific Party, 1996b. Site 974. *In* Comas, M.C., Zahn, R., Klaus, A., et al., *Proc. ODP, Init. Repts.*, 161: College Station, TX (Ocean Drilling Program), 55–111.

Takahashi, T., Broecker, W.S., Bainbridge, A.E., and Weiss, R.F., 1980. *Carbonate Chemistry of the Atlantic, Pacific, and Indian Oceans: The Results of the GEOSEC Expeditions, 1972–1978.* Lamont-Doherty Geol. Observ. Tech. Rep. 1, CV-1–80.

Tribble, J.S., and Wilkens, R.H., 1994. Microfabric of altered ash layers, ODP Leg 131, Nankai Trough. *Clays Clay Miner.*, 42:428–436.

Tribble, J.S., Wilkens, R., Arvidson, R.S., and Busing, C.J., 1993. Sediments of the Hawaiian Arch: X-ray mineralogy and microfabric. *In* Wilkens, R.H., Firth, J., Bender, J., et al., *Proc. ODP, Sci. Results*, 136: College Station, TX (Ocean Drilling Program), 65–76.

Wilkens, R.H., De Carlo, E.H., and Tribble, J.S., 1992. *Data report:* X-ray bulk mineralogy of Exmouth and Wombat Plateau sediments, northwest Australian margin. *In* von Rad, U., Haq, B.U., et al., *Proc. ODP, Sci. Results*, 122: College Station, TX (Ocean Drilling Program), 887–896.

Wilkens, R.H., Schreiber, B.C., Caruso, L., and Simmons, G., 1987. The effects of diagenesis on the microstructure of Eocene sediments bordering the Baltimore Canyon Trough. *In* Poag, C.W., Watts, A.B., et al., *Init. Repts. DSDP*, 95: Washington (U.S. Govt. Printing Office), 527–547.

Date of initial receipt: 7 May 1997
Date of acceptance: 26 January 1998
Ms 161SR-252